

DELAMINATION ANALYSIS OF COMPOSITES USING A FINITE ELEMENT BASED DISCRETE DAMAGE ZONE MODEL

Xia Liu, Ravindra Duddu, Haim Waisman
Columbia University
610 Seeley W. Mudd Building, 500 West 120th Street
New York, NY 10027

ABSTRACT

We perform delamination analysis in laminated composites in 2D and 3D using the discrete damage zone model within the framework of the finite element method. In this approach, spring-like elements are placed at the laminate interface and damage laws are used to prescribe both interfacial spring softening and bulk material stiffness degradation to study crack propagation. The irreversibility of damage naturally accounts for the subsequent reduction of material stiffness once the material is loaded beyond the elastic limit. The model is implemented in the commercially available ABAQUS software via the user element subroutine (UEL). Numerical results for 2D mixed-mode and 3D mode-I delamination are presented. The results for the benchmark examples show good agreement with those obtained from virtual crack closure technique (VCCT), which validates the method. This discrete method is particularly suitable when the material nonlinearities in the continuum surrounding the crack tip are significant.

1. INTRODUCTION

Delamination and debonding are the two major failure modes in laminated composites [1], but, often damage may accumulate in the weaker matrix leading to matrix cracking. Therefore, specialized methods are needed for the numerical analysis of fracture and delamination in composites so as to obtain reasonable results. To this end, we have recently proposed a discrete damage zone model within the frame of the finite element (FE) method that is further explored herein. This method falls into the class of the cohesive zone models (CZMs), however, it is different from the widely popular continuum cohesive zone models (CCZMs), which is addressed later in this section.

The numerical approaches used to study fracture and delamination in composites may be broadly classified into: (i) linear elastic fracture mechanics (LEFM) based [2, 3] and (ii) the cohesive zone modeling based. The LEFM approaches have been widely used to tackle delamination problems due to its simplicity and effectiveness [4– 6]; however, such an approach requires an initial crack and a negligible size of nonlinear zone at the crack tip [7]. In order to overcome these limitations, the cohesive zone modeling approach was proposed initially by Barenblatt and Dugdale [8, 9]. The concept introduces a bounded stress within the cohesive zone at the crack tip. This method has been widely used in simulations for composite materials and dynamic crack growth [10–13]. However, there are some inevitable computational issues associated with the CCZMs, such as the shape of the softening region of the cohesive laws and the integration scheme may cause convergence difficulties, oscillation and mesh sensitivity [11–13].

In order to deal with the computational issues associated with the CCZMs, discrete interfacial spring elements were introduced by Cui and Wisnom [14], instead of continuum cohesive elements. Later, Xie and Waas [15, 16] developed this idea by proposing the discrete cohesive zone model (DCZM), which employs bilinear traction-separation laws as constitutive laws in the discrete spring elements at the finite element nodes of the interface. Their approach is shown to overcome the computational issues of the continuous CZMs. However, this discrete cohesive zone model does not consider the material nonlinearities in the continuum finite elements surrounding the crack tip and so it precludes matrix cracking as a failure mode. Further, this DCZM has only been tested for bilinear traction separation laws and the corresponding negative tangent stiffness of the interface element may lead to convergence issues.

The current discrete damage zone model (DDZM) is different from the above mentioned models in three respects: (i) it employs spring-like elements at FE nodes whose softening behavior is given by a damage law; (ii) it considers damage of the surrounding continuum so as to include the effects of matrix cracking on the macroscopic mechanical behavior; and (iii) it uses the non-negative secant modulus in order to avoid convergence issues. The DDZM defines the force-separation law of the interfacial spring elements based on continuum damage mechanics and not particularly from any cohesive zone model. For homogeneous isotropic material, the same damage law is implemented in both the interfacial spring and bulk continuum elements; whereas, for a laminated composite, the damage law or parameters may be different in the springs and in the continuum. This paper is organized as follows: Section 2 describes the DDZM formulation, the procedure for parameter identification and the numerical implementation. Section 3 presents the results for two benchmark examples involving 3D mode-I and 2D mixed-mode delamination and discusses their convergence to the LFM solution. In addition, we present results of fracture analysis under a three-point bending test to study fracture in adhesive joints. Section 4 details the conclusions and the directions of future research.

2. FORMULATION AND IMPLEMENTATION

2.1 Discrete Interface Element

The proposed DDZM is developed from the perspective of damage mechanics. Therefore, the material failure is interpreted as stiffness degradation due to damage evolution in both interface and bulk elements. Figure 1 shows a typical mesh for the double cantilever beam (DCB) with standard quadrilateral finite elements in the continuum and with interface elements at the finite element nodes along the interface. These interface elements are multi-dimensional spring like elements resisting displacement along and perpendicular to their axis. In this article, the analysis needs only two-dimensional springs and the implementation is detailed in Section 2.3.

Now, let us derive the force-separation law for a one-dimensional spring element by considering the damage model proposed by Mazars [17] for brittle materials,

$$D = 1 - (1 - A) \frac{\delta^{cr}}{\delta} - \frac{A}{\exp(B(\delta - \delta^{cr}))} \quad [1]$$

where D is the damage variable, A and B are parameters, δ is the interfacial separation, and δ^{cr} is the critical interface separation required to initiate damage. We assume the parameter $A = 1.0$

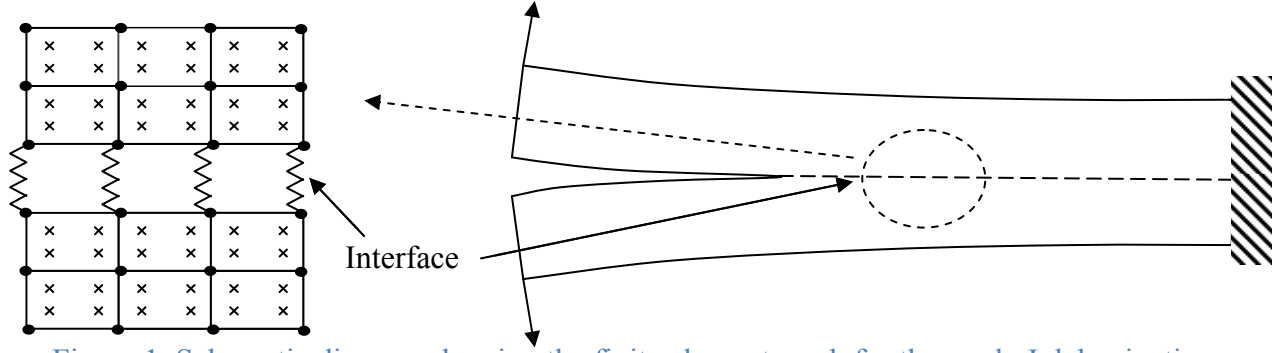


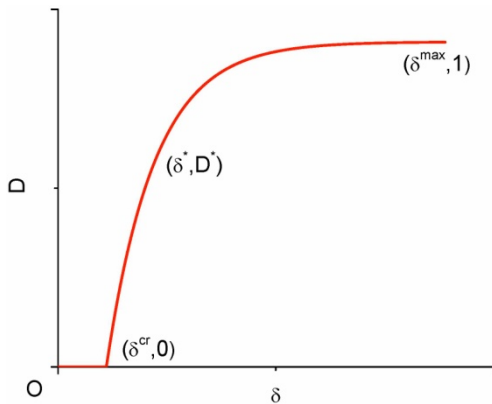
Figure 1. Schematic diagram showing the finite element mesh for the mode-I delamination analysis of a double cantilever beam. The 'x's indicate the integration (Gauss) points and the dots indicate the finite element nodes and the dashed line indicates the delamination surface.

for simplicity of the expressions without loss of generality. The behavior of this damage model is shown in Figure 2(a). Using equation 1, the force–separation ($F - \delta$) relation at a point $\delta^* \in (\delta^{cr}, \delta^{max})$, may be written from the $F - \delta$ curve's geometry shown in Figure 2(b) as,

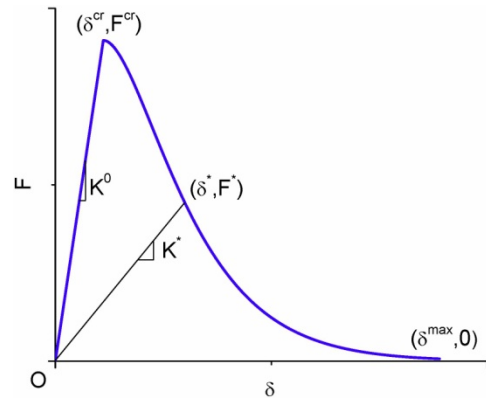
$$F^* = K^* \delta^* = (1 - D)K^0 \delta^* = \frac{K^0 \delta^*}{\exp(B(\delta^* - \delta^{cr}))} \quad [2]$$

where K^0 is the initial undamaged stiffness of the spring and δ^{max} is the maximum separation in the spring just before complete failure (rupture). Note that for the current exponential model $\delta^{max} = \infty$. Thus, the general one-dimensional force–separation law in the spring element with exponential softening is given by,

$$F = \begin{cases} K^0 \delta, & \text{if } \delta \in [0, \delta^{cr}] \\ \frac{K^0 \delta}{\exp(B(\delta - \delta^{cr}))}, & \text{if } \delta \in (\delta^{cr}, \infty] \end{cases} \quad [3]$$



(a) Damage vs. separation



(b) Force vs. separation

Figure 2. The damage and mechanical behavior of the current discrete interface element.

Thus, the procedure to derive the force-separation law from a given damage model is straightforward. The behavior of the springs in multi-dimensions can be similarly written for each directional component assuming there is no interaction between the normal and tangential components. Then, the interaction under mixed-mode fracture can be incorporated using the combined fracture energy criterion, which is detailed in the Section 2.4. In this article, we consider only Mazars damage model, however, the formulation is general and other damage models may also be employed to derive appropriate force–separation laws.

2.2 Parameter Identification

The parameters that need to be identified include the critical separation for damage initiation, δ^{cr} , the undamaged spring stiffness, K^0 , and the damage coefficient, B , along and perpendicular to the axis of the spring. Now, let us consider a 2D interface element and determine the parameters from the three principles of linear elastic fracture mechanics. First, the spring forces along (normal) and perpendicular (tangential) to its axis are maximum when the corresponding separations reach the critical values, that is,

$$\left. \frac{dF_n}{d\delta_n} \right|_{\delta_n=\delta_n^{cr}} = 0 \quad [4]$$

$$\left. \frac{dF_t}{d\delta_t} \right|_{\delta_t=\delta_t^{cr}} = 0 \quad [5]$$

where the subscripts n, t denote the normal and tangential components, respectively. Second, the maximum tractions (T_n, T_t) correspond to the respective cohesive strengths (σ_{max}, τ_{max}),

$$T_n|_{\delta_n=\delta_n^{cr}} = \lim_{\Delta a \rightarrow 0} \left. \frac{F_n}{\Delta a} \right|_{\delta_n=\delta_n^{cr}} = \sigma_{max} \quad [6]$$

$$T_t|_{\delta_t=\delta_t^{cr}} = \lim_{\Delta a \rightarrow 0} \left. \frac{F_t}{\Delta a} \right|_{\delta_t=\delta_t^{cr}} = \tau_{max} \quad [7]$$

Owing to the finite element discretization, the force in each spring acts on an area of Δa , which depends on the characteristic size of the mesh. Third, the areas under the normal and tangential force–separation curves should correspond to the mode-I and mode-II critical fracture energy release rates, that is,

$$\int_0^{\delta_n^{max}} T_n(\delta_n, 0) d\delta_n = \int_0^{\delta_n^{max}} \frac{F_n(\delta_n)}{\Delta a} d\delta_n = G_{IC} \quad [8]$$

$$\int_0^{\delta_t^{max}} T_t(\delta_t, 0) d\delta_t = \int_0^{\delta_t^{max}} \frac{F_t(\delta_t)}{\Delta a} d\delta_t = G_{IIC} \quad [9]$$

Using the above six equations 4–9, we can calibrate the six parameters of the exponential softening law, B_n , δ_n^{cr} , K_n^0 , B_t , δ_t^{cr} and K_t^0 in 2D. The final expressions for the parameters after some mathematical simplification are,

$$\delta_n^{cr} = \frac{G_{IC}}{\sigma_{max} \exp(1)} ; \delta_t^{cr} = \frac{G_{IIC}}{\tau_{max} \exp(1)} \quad [10]$$

$$B_n = \frac{1}{\delta_n^{cr}} ; B_t = \frac{1}{\delta_t^{cr}} \quad [11]$$

$$K_n^0 = B_n^2 \Delta a \frac{G_{IC}}{\exp(1)} ; K_t^0 = B_t^2 \Delta a \frac{G_{IIC}}{\exp(1)} \quad [12]$$

2.3 Numerical Implementation

In this section, we shall describe briefly the numerical implementation of the discrete damage zone model within the framework of the finite element method. Let us consider the behavior around the crack tip as shown in Figure 3. Under an applied load, as the extensions of interface springs increase the interface separates and the crack opens. Eventually, under a sustained load this will lead to the complete failure of the springs. In Figure 3, spring 6 has completely failed whereas springs 1, 2 have zero extensions and so all these springs have zero force. The springs 3, 4, 5 have non-zero extensions and non-zero forces.

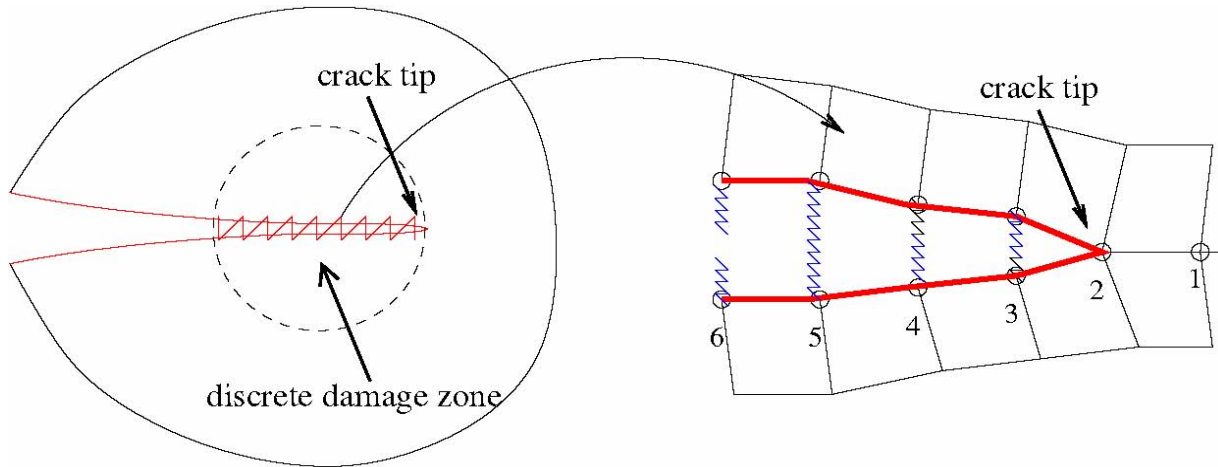


Figure 3. Sketch of the discrete damage zone model (DDZM) in a domain with an initial crack

In a general case scenario, when the point of fracture initiation in a domain is not known, every node of the finite element mesh is defined as double nodes and discrete spring elements are placed between these double nodes. For benchmark problems, the potential crack path is already known and hence there is no need to put springs in the whole domain. The proposed DDZM is implemented in the commercial finite element analysis software ABAQUS. The discrete spring elements are defined via the user defined element subroutine UEL. Figure 4 shows the element definition and node numbering convention. Even for the case of 3D delamination analysis, the

interface forces can be resolved into normal and tangential components and the following scheme can be implemented using the principles of vector and tensor calculus. For brevity and simplicity, we describe the implementation for a general 2D spring element that is not aligned with the global coordinate axes. Note that the initial length of these spring elements is zero since the springs are attached between double nodes. After deformation, the displacement vector in global Cartesian coordinates (x_1, x_2) is given by,

$$\mathbf{u} = (u_1, u_2, u_3, u_4)^T \quad [13]$$

In local coordinates (x'_1, x'_2) , the vector is given as,

$$\mathbf{u}' = \mathbf{R}\mathbf{u} = (u'_1, u'_2, u'_3, u'_4)^T \quad [14]$$

where a “ T ” in the superscript denotes transpose and \mathbf{R} is the anticlockwise rotation matrix is given by,

$$\mathbf{R} = \begin{bmatrix} \cos\theta & \sin\theta & 0 & 0 \\ -\sin\theta & \cos\theta & 0 & 0 \\ 0 & 0 & \cos\theta & \sin\theta \\ 0 & 0 & -\sin\theta & \cos\theta \end{bmatrix} \quad [15]$$

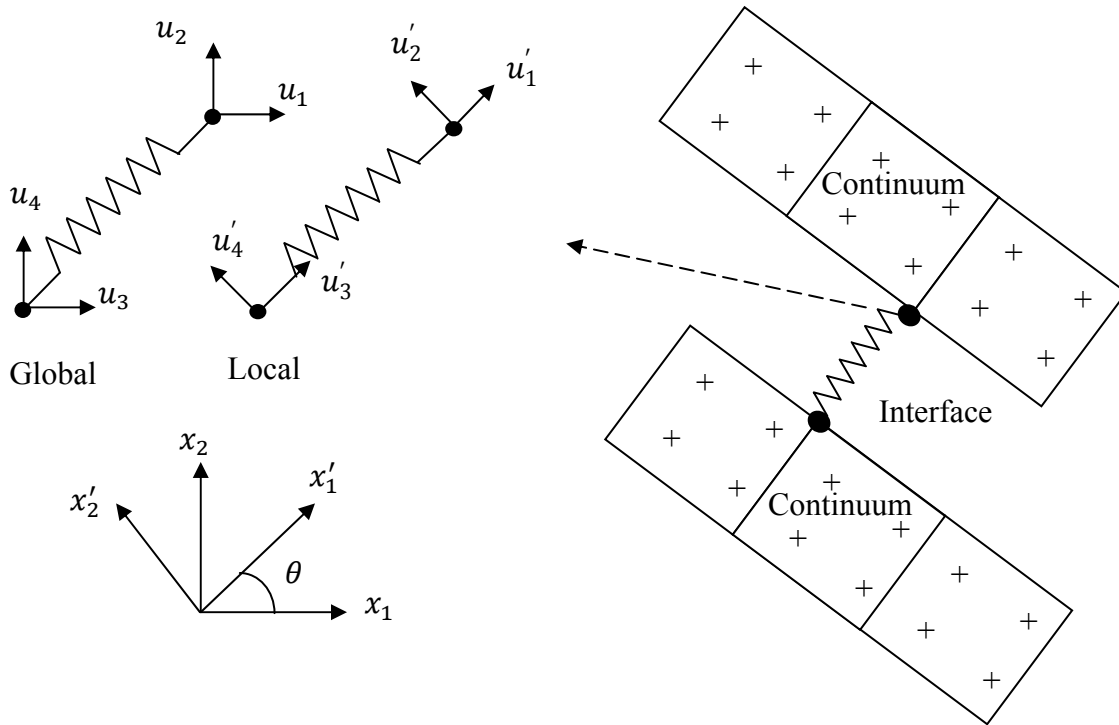


Figure 4. Sketch of the discrete spring element placed at the nodes of the continuum elements at the interface and the definition of degrees of freedom in local and global coordinates. The inclination of the spring θ defines the angle of coordinate rotation.

The stiffness of the spring is a function of damage variable D in both directions, along (n) and perpendicular (t) to its axis,

$$K_n = (1 - D_n)K_n^0 \quad [16]$$

$$K_t = (1 - D_t)K_t^0 \quad [17]$$

Note that the above two equations give the expressions for the non-negative secant moduli, which avoid the convergence issues associated with the possibly negative tangent moduli. In order to implement this interface element via ABAQUS user element subroutine UEL, the element stiffness matrix, \mathbf{K} (AMATRX), and the residual force vector, \mathbf{r} (RHS), in global coordinates need to be defined. The corresponding expressions are given by,

$$\mathbf{r}' = \mathbf{R}^T \begin{Bmatrix} -K_n(u'_1 - u'_3) \\ -K_t(u'_2 - u'_4) \\ K_n(u'_1 - u'_3) \\ K_t(u'_2 - u'_4) \end{Bmatrix} \quad [18]$$

$$\mathbf{K} = \mathbf{R}^T \begin{bmatrix} K_n & 0 & -K_n & 0 \\ 0 & K_t & 0 & -K_t \\ -K_n & 0 & K_n & 0 \\ 0 & -K_t & 0 & K_t \end{bmatrix} \mathbf{R} \quad [19]$$

Note that, in addition to UEL subroutine for the discrete element, we have implemented the user material subroutine UMAT for incorporating damage in the continuum elements. A scalar damage variable is used to implement Mazars damage in the continuum. Again, for brevity, the numerical implementation of the UMAT is omitted in this section since it is quite straightforward.

2.4 Mixed-Mode Fracture Criterion

In most of the engineering applications, delamination involves both mode-I and mode-II opening. Therefore, we need to specify the failure based on mixed-mode fracture energy criterion. Herein, we use a linear criterion for mixed-mode interaction, previously suggested by Wu and Reuters [19], is given by,

$$\frac{G_I}{G_{IC}} + \frac{G_{II}}{G_{IIC}} = 1.0 \quad [20]$$

where G_I and G_{II} are evaluated as,

$$G_I = \int_0^{\delta_n} \frac{F_n(\delta_n)}{\Delta a} d \delta_n \quad ; \quad G_{II} = \int_0^{\delta_t} \frac{F_t(\delta_t)}{\Delta a} d \delta_t \quad [21]$$

If the criterion in equation 20 is met for an interface element, then we consider that it has failed and the damage in the spring is set as $D_n = D_t \approx 1.0$.

3. NUMERICAL EXAMPLES AND RESULTS

In this section, we present three examples including one benchmark examples of 2D mixed-mode fracture known as the single leg bending (SLB) problem [18]. A convergence study is performed for the SLB problem to show the influence of cohesive strength in comparison to the results obtained from LEFM. The other two examples include 3D mode-I delamination in a double cantilever beam (DCB) problem and fracture at adhesive joints in a simply supported beam (SSB) problem. Table 1 summarizes the material properties used in each example. The SLB problem specimen consists multiple layers made of two different composite materials (L_1 and L_2) and the SSB problem compares a weak and strong interface, as given in Table 1.

Table 1. Summary of material properties used in each example.

Material	E_{11} (N/mm ²)	E_{22} (N/mm ²)	ν_{12}	G_{IC} (N/mm ¹)	σ_{max} (N/mm ²)	G_{IIC} (N/mm ¹)	τ_{max} (N/mm ²)
SLB (L_1)	9.1e6	1.5e6	0.51	5.6	2.0e3	9.3	5.0e3
SLB (L_2)	2.5e6	1.5e6	0.14	5.6	2.0e3	9.3	5.0e3
DCB (3D)	8.00e6	8.00e6	0.00	1.2	4.0	-	-
SSB (weak)	2.4e3	2.4e3	0.25	3.0	3.3e1	3.0	3.3e1
SSB (strong)	2.4e3	2.4e3	0.25	3.0e2	3.3e2	3.0e2	3.3e2

3.1 2D Mixed-Mode Delamination: Single Leg Bending

Herein, we validate and illustrate the convergence of the DDZM for mixed-mode delamination. The set up of the single leg bending (SLB) benchmark problem is shown in Figure 6. The beam is simply supported at the left and right ends. A crack of length a_0 is prescribed as shown so as to initiate delamination. The dimensions of the beam are as follows: $a_0 = 0.27$ mm, $H_1 = 0.0884$ mm, $H_2 = 0.2876$ mm, $L_1 = 3.0$ mm, $L_2 = 4.8$ mm, $L = 6.0$ mm.

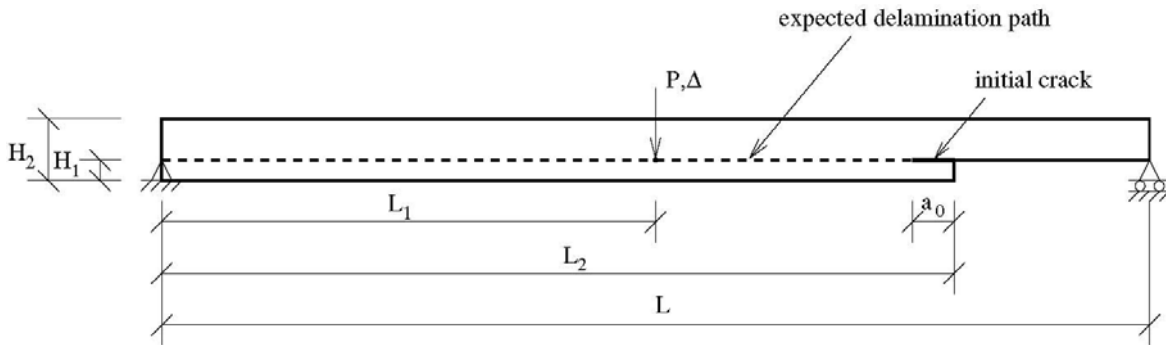
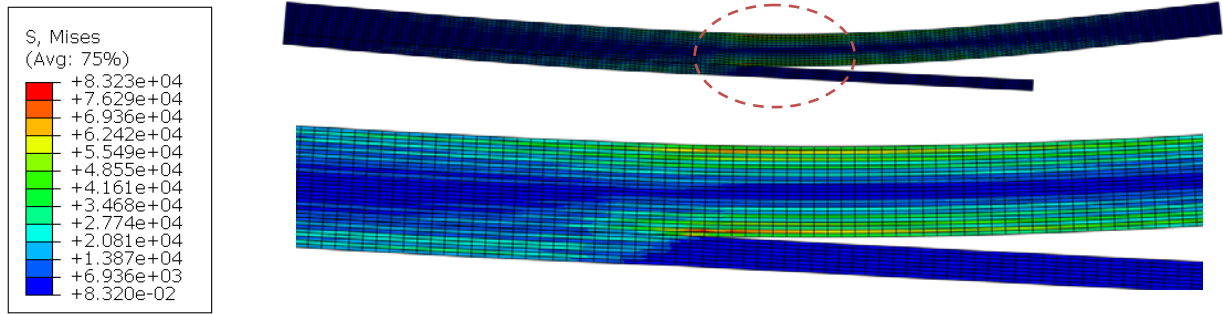
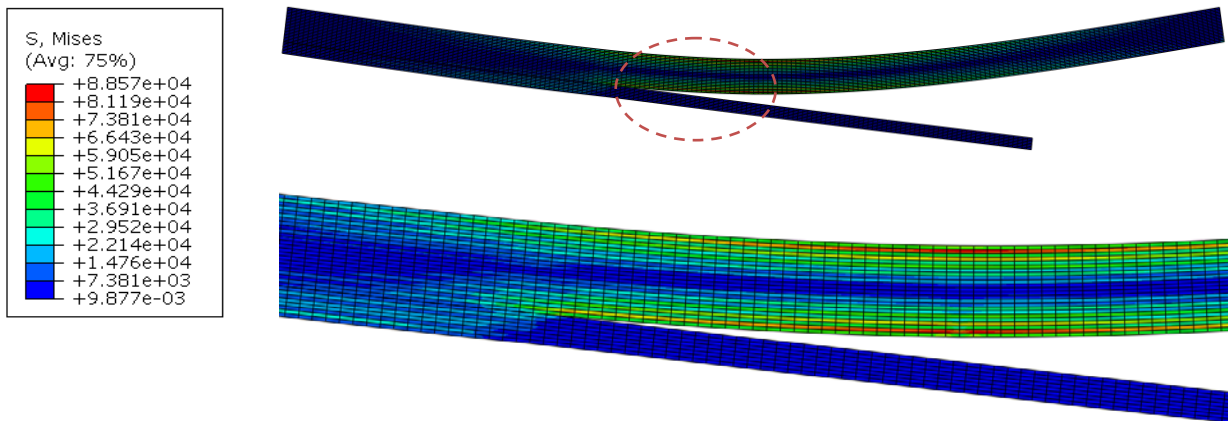


Figure 5. Initial geometry and boundary conditions for single leg bending (SLB) model

To initiate mixed mode delamination, displacement increments are applied at mid-span as shown in the Figure 5. Note that displacement control is applied in order to capture the softening behavior of the load–displacement ($P-\Delta$) curve. The discrete spring elements are placed only along the dashed line, which describes the expected delamination path. Figures 6(a) and 6(b) show the Mises contour plots on deformed shape at time step “A” when the crack propagates to the point of load application and at the final time step “B” of the simulation. It can be seen from Figure 6 that once the lower layer separates it is under zero.



(a) Time step A when the crack propagates to the point of load application



(b) The final time step B of the simulation

Figure 6. Mises contour plot on deformed shape at the application point and the end of the simulation. The area circled by red dashed line is zoomed in to show the finite element mesh.

Figure 7 shows the $P-\Delta$ curves and the behavior at time steps A and B are marked. As the beam deforms under the applied loading, the extensions (δ) in the interface elements increase and eventually when a critical displacement is reached, the crack propagates very quickly so as to cause an abrupt drop in the load bearing capacity of the beam. This sudden drop in load bearing capacity happens till the crack reaches the application point of load at time step A. From this point, the crack propagates much slower and the behavior of the beam is close to linear elastic with a different slope than at the beginning. This behavior can be clearly observed in Figure 7. Results obtained from the virtual crack closure technique (VCCT) are used as reference LEM solutions. The results from the DDZM are in good agreement with those of VCCT, which

validates our implementation; however, the DDZM results depict a slightly less abrupt failure than the VCCT results owing to bounded stress in the cohesive zone.

Next, in order to demonstrate the convergence of the scheme, we vary the material cohesive strengths one component at a time. In the results of Figure 7(a) the normal cohesive strength σ_{max} is a constant while in those of Figure 7(b) the tangential cohesive strength τ_{max} is a constant. The numerical results obtained from higher cohesive strengths converge to the VCCT results demonstrating the convergence of the DDZM to the LEFM solution.

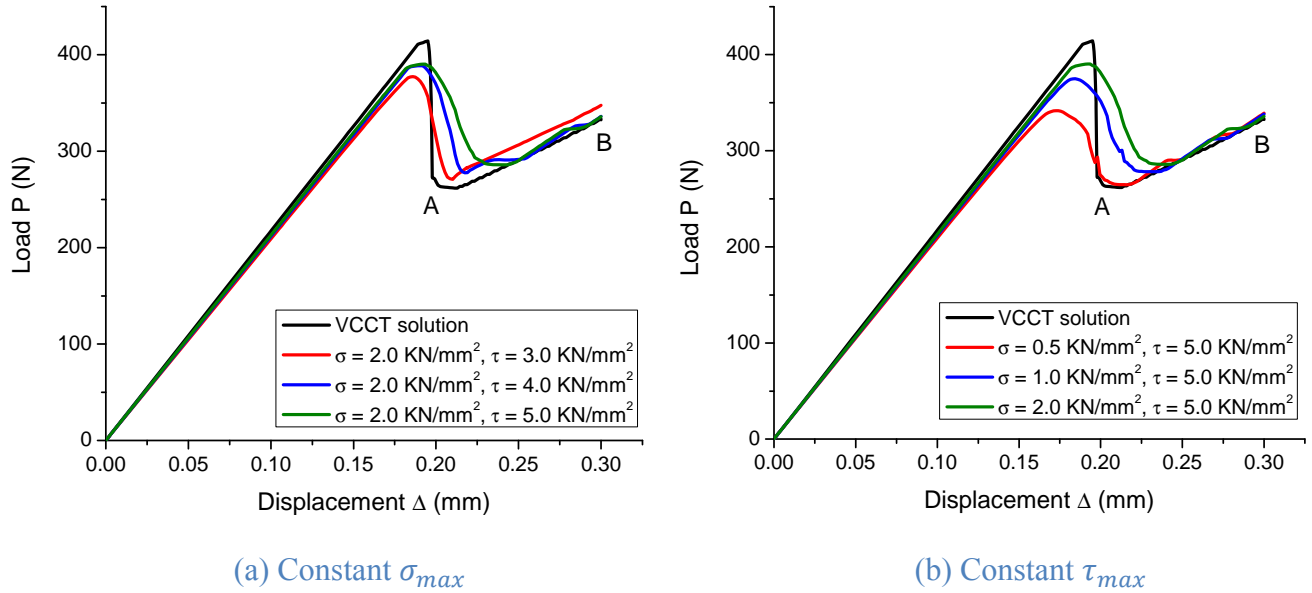


Figure 7. The load vs. displacement curves for the single leg bending problem. The results for higher cohesive strengths demonstrate convergence to the LEFM solution.

3.2 3D Mode-I Delamination: Double Cantilever Beam

Herein, we demonstrate the applicability of the DDZM for mode-I delamination analysis in 3D. The initial geometry and boundary conditions are shown in Figure 8. The right end of the beam is fixed and displacement boundary conditions are applied on both the upper and lower layers at mid-point on the left end. Each layer is a 2D plate with zero thickness. The dimensions are as follows: $W = 1$ mm, $L = 9$ mm.

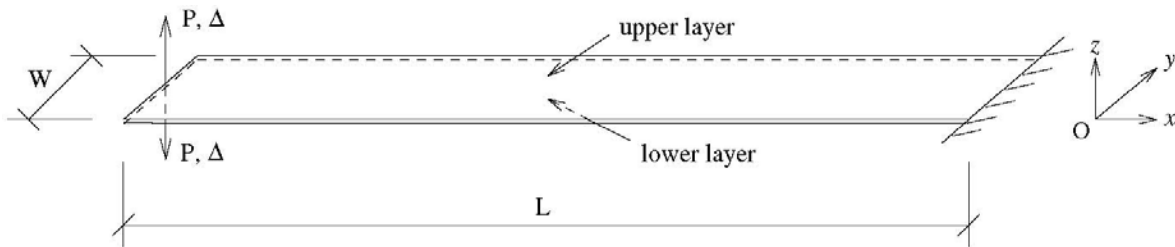
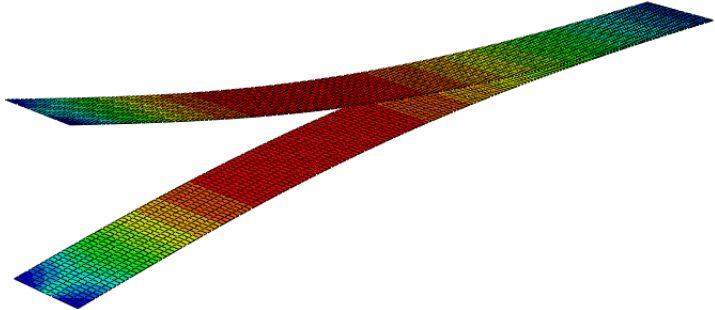
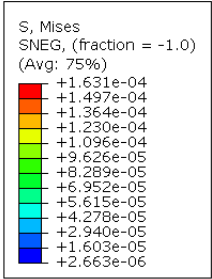
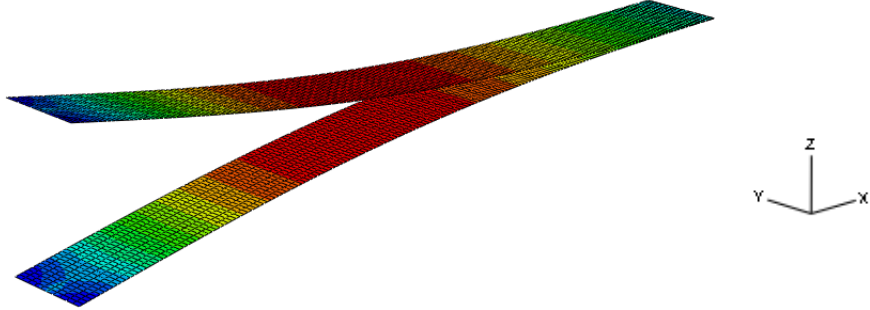
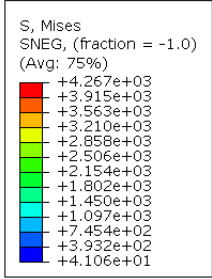


Figure 8. Initial geometry and boundary conditions for double cantilever bending (DCB) in 3D

The delamination occurs due to the debonding of the upper and lower layers. The discrete spring elements are placed between these two layers by connecting double nodes belonging to each layer. Again, displacement control is used so as to capture the global softening behavior. Figure 9(a) and 9(b) show the Mises contour plots on deformed shape at the end of the first and last time steps of the simulation, respectively. Upon close observation, one can see the variation of the stress in the y-direction close to the left edge. This is the effect of a local stress concentration as the displacement increments are applied at the mid-point of the edge. Far away from the point of application, the stress is uniform across the width of the specimen.



(a) Delamination at the end of the first time step



(b) Delamination at the end of the final time step

Figure 9. Mises contour plot on deformed shape of double cantilever bending in 3D

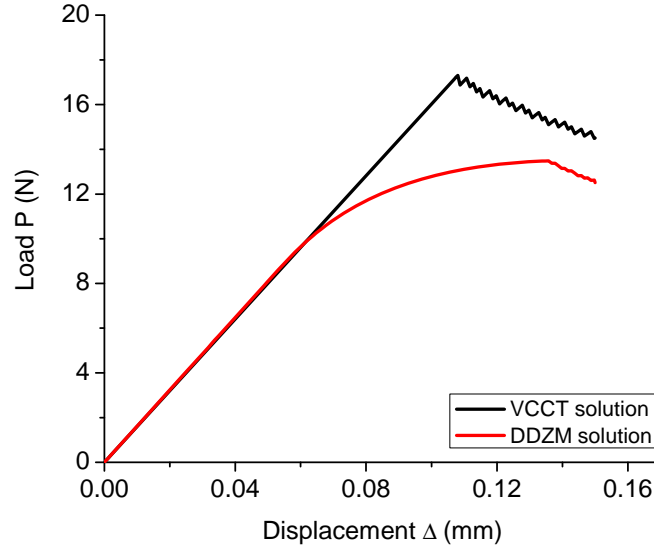


Figure 10. Load vs. displacement curves for double cantilever beam (DCB) debonding in 3D

The load-displacement ($P-\Delta$) curve obtained from the DDZM is plotted against the result from VCCT, shown in Figure 10. The VCCT result consists of a linear regime followed by a failure regime exhibiting small fluctuations in load bearing capacity, whereas, the DDZM result depicts a smoother global failure curve. This is expected since the DDZM assumes a cohesive zone with damageable interface elements wherein the individual elements gradually failure while simultaneously redistributing the forces to the surrounding active interface elements.

3.3 Mode-I fracture: Simply Supported Beam Bending

Herein, we consider mode-I fracture of an adhesive joint in a beam element using the DDZM. The initial geometry and boundary conditions for this simply supported beam are shown in Figure 11. Both the initial crack and the load are prescribed at mid-span. Displacement boundary condition is applied in order to deform the beam. The dimensions are as follows: $a_0 = 10$ mm, $H = 20$ mm, $L_1 = 45$ mm, $L_2 = 22.5$ mm, $L = 90$ mm.

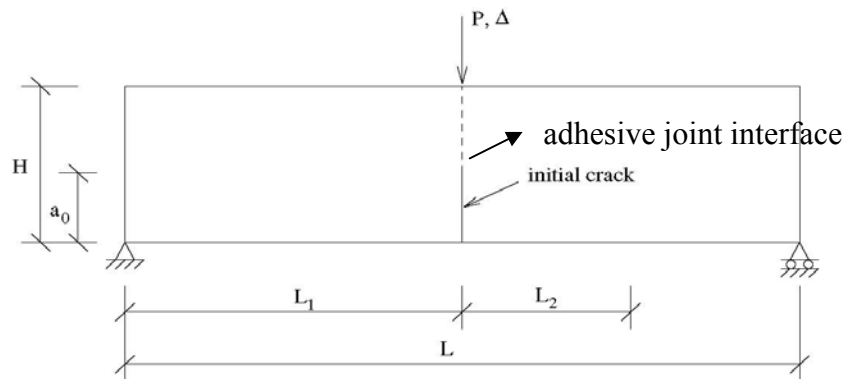
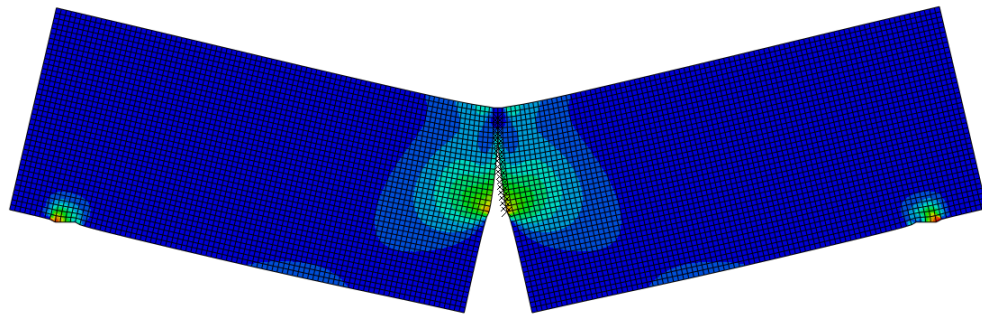
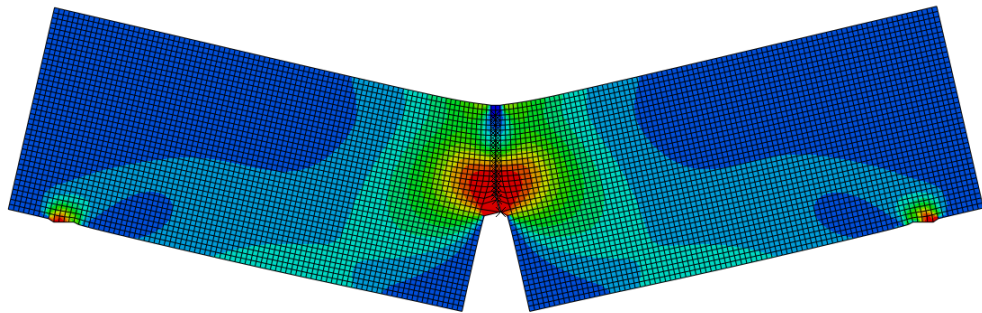


Figure 11. Initial geometry and boundary conditions for simply supported beam (SSB). The adhesive joint interface is indicated by the dashed line.

The discrete spring elements are placed along the adhesive joint interface described by the dashed line in Figure 11. Mazars damage law [17] governs the behavior of both the interface and continuum elements. We consider two hypothetical cases, one with weak interface and the other with strong interface. The materials properties assumed are given in Table 1. Damage contour plots for these two cases are shown in Figure 12. For a weak interface the failure occurs primarily in the interface elements, whereas, for a strong interface the damage occurs in the continuum elements surrounding the crack tip.



Case I: weak interface (hypothetical)



Case II: strong interface (hypothetical)

Figure 12. Damage contour plots for both weak interface and strong interface. The red areas indicate completely damaged elements.

The DDZM is able to capture both interface failure in the adhesive joint as well as the failure of surrounding matrix due to microcracking. Thus, this example illustrates the generality of the current approach.

4. CONCLUSIONS

4.1 Summary

The discrete damage zone model (DDZM) [20] has been implemented to study delamination in laminated composites. The model has been developed from the perspective of damage mechanics and so it naturally accounts for the irreversibility of stiffness degradation once the material is loaded beyond the elastic limit. The model considers both damage of the continuum and the interface and so it is able to capture multiple failure modes such as debonding and matrix

cracking. For a homogeneous isotropic material the same damage law governs both the interface element and continuum element stiffness degradation, thus, leads to a unified formulation. Further, since damage evolution is allowed in both interfacial and bulk elements, the model is applicable to problems where the point of fracture initiation and the path of fracture propagation are not known a priori.

This generalized formulation is simple and can be readily incorporated into existing finite element software such as ABAQUS. The numerical results, of 2D mixed-mode single leg beam bending and 3D double cantilever beam mode-I delamination, from the DDZM show good agreement with the reference VCCT results. Moreover, the numerical investigation of the mixed mode single leg bending test with various cohesive strengths demonstrates the convergence to linear elastic fracture mechanics. The results of mode-I fracture of adhesive joint interface in beam elements demonstrate the versatility of the method for problems involving multiple modes of failure. Thus, the study conducted in the article illustrates the viability of the method for study failure in laminated composites which is important to predict their durability and performance.

4.2 Afterwords

The irreversibility of damage makes this numerical scheme particularly suitable for studying fatigue behavior of composites. By decomposing the total damage into static and cyclic components and by defining the corresponding damage laws we can investigate failure under fatigue loading. Currently, we are working on extending the discrete damage zone model.

5. REFERENCES

1. Robinson, P., Besant, T. & Hitchings, D., "Delamination growth prediction using a finite element approach." 2nd ESIS TC4 Conference on Polymers and Composites, Les Diablerets, Switzerland, 1999
2. Griffith, A.A., "The phenomena of rupture and flow in solids." *Philosophical Transactions of the Royal Society*, London, Series A, 221(1921): 163-198
3. Irwin, G.R., "Analysis of stresses and strains near the end of a crack traversing a plate." *Journal of Applied Mechanics*, 24(1957): 361-364
4. Blackman, B., Dear, J.P., Kinloch, A.J. & Osiyemi, S., "The calculation of adhesive fracture energies from double-cantilever beam test specimens." *Journal of Materials Science Letters*, 10(1991): 253-256
5. Blackman, B.R.K., Kinloch, A.J., Paraschi, M. & Teo, W.S., "Measuring the mode I adhesive fracture energy, G_{IC} , of structural adhesive joints: the results of an international round-robin." *International Journal of Adhesion & Adhesives*, 23(2003): 293-305
6. Blackman, B.R.K., Hadavinia, H., Kinloch, A.J., Paraschi, M. & Williams, J.G., "The calculation of adhesive fracture energies in mode I: Revisiting the tapered double cantilever beam (TDCB) test." *Engineering Fracture Mechanics*, 70(2003): 233-248
7. Bazant, Z.P., "Size effect on structural strength: A review." *Archives of Applied Mechanics*, 69(9-10)(1999): 703-725

8. Dugdale, D.S., "Yielding of steel sheets containing slits." *Journal of the Mechanics and Physics of Solids*, 8(2)(1960): 100-104
9. Barenblatt, G.I., "The mathematical theory of equilibrium cracks in brittle fracture." *Advances in Applied Mechanics*, 7(1962): 55-129
10. Fish, J., Yu, Q. & Shek, K.L., "Computational damage mechanics for composite materials based on mathematical homogenisation." *International Journal for Numerical Methods in Engineering*, 45(1999): 1657-1679
11. de Borst, R., "Some recent issues in computational failure mechanics." *International Journal for Numerical Methods in Engineering*, 52(2001): 63-95
12. de Borst., R., "Numerical aspects of cohesive-zone models." *Engineering Fracture Mechanics*, 70(2003): 1743-1757
13. Mi, Y., Cisfield, M.A., Davies, G.A.O. & Hellweg, H.B., "Progressive delamination using interface elements." *Journal of Composite Materials*, 32(1998): 1246-1272
14. Cui, W.C. & Wisnom, M.R., "A combined stress-based and fracture mechanics-based model for predicting delamination in composites." *Composites*, 24(6)(1993): 467-474
15. Xie, D., Salvi, A.G., Sun, C. & Waas, A.M., "Discrete cohesive zone model to simulate static fracture in 2D triaxially braided carbon fiber composites." *Journal of Composite Materials*, 40(22)(2006): 2025-2046
16. Xie, D. & Waas, A.M., "Discrete cohesive zone model for mixed-mode fracture using finite element analysis." *Engineering Fracture Mechanics*, 73(2006): 1783-1796
17. Mazars, J., "A description of micro and macro scale damage of concrete structures." *Engineering Fracture Mechanics*, 25(1986):729-737
18. Davidson, B.D., Kruger, R. & Konig, M., "Three-dimensional analysis of center-delaminated unidirectional and multidirectional single-leg bending specimens." *Composites Science and Technology*, 54(1995): 385-394
19. Wu, E. M. and Reuter, R. C., "Crack extension in fiberglass reinforced plastics." *University of Illinois TAM Report No. 275*, 1965
20. Xia, L., Duddu, R. and Waisman, H., "A discrete damage zone model for mixed-mode fracture initiation and propagation." *Engineering Fracture Mechanics*, in review